Effects of morphology in controlling propagation of density currents in a reservoir using uncalibrated three-dimensional hydrodynamic modeling

Behnam Zamani,[1*] Manfred Koch,[1] Ben R. Hodges[2]

[1]Department of Geohydraulics and Engineering Hydrology, Faculty of Civil and Environmental Engineering, University of Kassel, Germany; [2]Department of Civil, Architectural, and Environmental Engineering, University of Texas at Austin, TX, USA

ABSTRACT

In this study, effects of basin morphology are shown to affect density current hydrodynamics of a large reservoir using a three-dimensional (3D) hydrodynamic model that is validated (but not calibrated) with *in situ* observational data. The AEM3D hydrodynamic model was applied for 5-month simulations during winter and spring flooding for the Maroon reservoir in southwest Iran, where available observations indicated that large-scale density currents had previously occurred. The model results were validated with near-bottom water temperature measurements that were previously collected at five locations in the reservoir. The Maroon reservoir consists of upper and lower basins that are connected by a deep and narrow canyon. Analyses of simulations show that the canyon strongly affects density current propagation and the resulting differing limnological characteristics of the two basins. The evolution of the Wedderburn Number, Lake Number, and Schmidt stability number are shown to be different in the two basins, and the difference is attributable to the morphological separation by the canyon. Investigation of the background potential energy (BPE) changes along the length of the canyon indicated that a density front passes through the upper section of the canyon but is smoothed into simple filling of the lower basin. The separable dynamics of the basins has implications for the complexity of models needed for representing both water quality and sedimentation.

INTRODUCTION

Reservoirs, as artificial lakes, have characteristics and behaviors that differentiate them from most natural lakes due to rift-like depths and downstream flow controls (Ford and Johnson 1986). The assessment and prediction of physical and bio-geochemical processes (hereafter *biochemical* for simplicity) and their causes within reservoirs are important for both operations and environmental issues. Physical processes are drivers and controls of biochemical processes and play a key role in ecosystem behaviors. Among the former, the most important ones are hydrodynamic processes which dictate

the stratification and mixing that control the temporal and spatial distribution of nutrients and dissolved oxygen (Vincent *et al.*, 1991; Hamilton and Schladow, 1997; Schladow and Hamilton, 1997; Löffler, 2004).

Although hydrodynamics and water quality for natural lakes is a well-studied subject, and much of the research carried out up to date is applicable for issues common to both lakes and reservoirs (Jørgensen *et al.*, 2005), specific differences between the characteristics of natural lakes and reservoirs (*e.g.* being embedded in river networks where natural geology would not allow impoundment, the location of deepest portions, water release locations) leave a range of issues where the natural lake literature does not provide much guidance (USACE, 1987; Hayes *et al.*, 2017). One primary difference is that reservoirs are geologically "young," which leads to geological complexities that would be smoothed by centuries or millennia of sedimentation and erosion in a natural lake. As a result, reservoirs have morphologic complexities that often lead to deeper depths, steeper slopes, and long water residence times.

Numerous morphometric parameters, *e.g.* bathymetry, volume, area and depth, are controlling limnological and hydrodynamic characteristics of a reservoir and directly affect hydrodynamic processes, oxygen exchange, nutrient cycles and other water quality-related biochemical processes. The morphometric parameters are mutually connected, and their assessment provides insight into the present and likely future status of a reservoir. Reservoirs are typically located to maximize water storage for a minimum dam area, which typically results in deeper depths, stronger stratification, and different limnological indices than those of natural lakes in the

same region (Kennedy *et al.*,1985; Thornton *et al.*, 1996). From a hydrological perspective, many reservoirs are the water sink for a larger watershed than a natural lake of similar size (Ji, 2008), which can result in higher nutrient and sediment inflows and strong seasonal variation. As a further complexity, reservoirs typically have controlled in-/outflows at various depths varying from surface to bottom (Ji, 2008), which can affect the stratification regime (Imberger and Patterson, 1990).

When a storm flood enters a stratified reservoir, unless its water has precisely the same density as the reservoir water, it forms a density current as an underflow, interflow, or overflow (Ford and Johnson, 1983). Density current behaviors, such as travel time throughout the reservoir, thickness of the current, dilution rates, current temperature, suspended sediment concentration and the consequent turbidity are affected by reservoir stratification and also have feedbacks that alter the stratification (Chung *et al.*, 2009; Cortés *et al.*, 2014). Unfortunately, the interplay between density currents, stratification, and internal processes of a reservoir cannot be quantified with simple analytical expressions and, thus, computational approaches are required. Numerical modeling of density-current hydrodynamics provides insight into how these currents interact with the stratification and mixing processes. Such insight can assist in developing reservoir operating procedures to reduce undesirable effects of inflows (*e.g.*, increase in stratification and longer residence time in the hypolimnion).

Hydrodynamic models are used to simulate the behavior of lakes and reservoirs under various forcing conditions. Different physical and biochemical aspects of reservoirs have been investigated and numerically modeled in several studies. Hodges *et al.* (2000) and Hodges *et al.* (2006) studied basin-scale internal waves and their uncertainties in stratified lakes and demonstrated the good ability of the 3D-hydrodynamic model in predicting the internal waves dynamics and mixed layer depth, even for coarse vertical resolutions. Botelho and Imberger (2007) and Hipsey *et al.* (2008) modeled pollutants fate and transport in reservoirs and lakes. Zamani *et al.* (2018) modeled the hydrological effects on the limnological processes in reservoirs. A considerable number of studies, *e.g.* Bournet *et al.* (1999), Chung *et al.* (2009), Marti *et al.* (2011), An *et al.* (2014), Cortes *et al.* (2014), Hogg *et al.* (2017) have investigated and modeled the propagation density currents in various stratified reservoirs, either at laboratory or geophysical scale.

However, the interplay between the dynamics of density currents and reservoir morphometry appears to have received not enough attention in the previous studies. Even in studies involving the lakes' morphometry, *e.g.,* multi-basin or dendritic lakes and reservoirs, the focus has been mostly on the analysis of the performance of the numerical model (*e.g.* Rueda and McIntyre, 2010) or the prediction of the distribution of the density currents or their resulting sedimentation (*e.g.* Kim and Kim, 2006; Scheu *et al.* 2018).

In this study we investigate and model how the morphology of a reservoir affects its hydrodynamics and propagation of density currents. The study object is the Maroon reservoir in southwest Iran. The Maroon reservoir consists of upper and lower basins that are connected through a narrow and deep canyon. We examine the different hydrodynamic behaviors in the basins under extreme events that are affected by the narrow canyon during a 5-month flooding period in 2011-12. During that time measurements of water temperature in the reservoir were taken by the local water authority, mainly in the upper basin, however, with only limited measurements in the lower basin. Although this limited data is insufficient for evaluating the physics of storm-driven density currents, such information is needed for reservoir managers to evaluate operational strategies. Notwithstanding these shortcomings, in this paper we show that this limited data is sufficient to validate an uncalibrated three-dimensional (3D) hydrodynamic model, allowing to get deeper insight in the physical processes taking place in the Maroon reservoir.

METHODS

Study area

The Maroon reservoir is located on the Maroon River in southwest Iran (Fig. 1). The Maroon dam is located 13 km northeast of Behbahan city. The reservoir provides storage of irrigation water, hydropower, and serves as flood control for the Maroon River, one of the large rivers in Iran with a long-term annual mean flow upstream of the Maroon reservoir of 47 m^3s^{-1}, although the flow in any year is seasonally variable. The maxima and minima of the monthly flow happen typically in April (snowmelt) and October, respectively, and the flooding season typically starts in December.

The Maroon reservoir and dam began operation in 2000, so the reservoir is a young lake from a limnological point of view (Ford and Johnson, 1986). The reservoir has a catchment area of 3840 km^2 in the Zagros Mountains. The mean depth of the Maroon reservoir (the ratio of full storage volume to surface area) is 49 m, which classifies it as a deep reservoir (Ji, 2008). The reservoir is formed in a valley with steep side slopes, especially in the upper reservoir, and can be conceptually divided into an upper and lower basin separated by a narrow and deep canyon (Fig. 1c). Of the 30 km of the reservoir's thalweg approximately 17 km extends over the upper basin. The major part of the upper basin is formed in the narrow and

long valley of the Maroon River, with a width ranging between 100 and 650 m (at the Normal Pool Level - NPL). The canyon connecting the two basins is 2400 m long, with a width ranging between 170 m and 350 m at NPL. Based on volume, thalweg length, and flows, the reservoir has a mean water residence time of 1.27 years.

The Maroon reservoir is classified as a *warm-monomictic* lake using the thermal classification of lakes suggested by Hutchinson and Löffler (1956). This implies a major stratification in summer and a major overturn and mixing period in winter. Most of the Iranian lakes and reservoirs, especially in our study region (Khuzestan province and Zagros region), are also in this category. The winter mixing period in the lakes and reservoirs of the study area is in December. In this time of the year the onset of the flooding period of the Maroon River occurs also, providing cold flood inflows into the reservoir due to cold winter precipitation. Simultaneously, air temperature and the solar radiation start to increase after January, so the stratification gradually develops in the reservoir water column.

Data

The nearest meteorological station is the Behbahan synoptic station, 13 km southwest of the Maroon dam, which provides meteorological data for this study. The data are available from 1994 as hourly records of air temperature, atmospheric pressure, wind, cloudiness and humidity, and are used to set the thermal and wind stress boundary conditions of the model. The solar (shortwave) radiation is not measured directly at the Behbahan station and, therefore, was estimated from the measured bright sunshine data using the FAO procedure (Allen *et al.*, 1998) for the station by implementing the Ångström coefficients (Ångström, 1924), calculated and validated for the region by Hajjam and Jamei (2009). Yang and Koike (2005) found underestimations of up to 10% in the calculated peaks of hourly solar radiation using this method in mountainous areas (in Japan). However, studies on the solar radiation in Iran (Alizadeh and Khalili, 2009, Hajjam and Jamei, 2009) found no significant difference between FAO - calculated and observed solar radiation values in Iran, including the present study area (Khuzestan province).

The river flow at the Eydanak station is available throughout the year as daily mean flows, with more frequent (hourly) measurements during the flooding seasons.

Continuously-measured water temperatures were available for the Maroon reservoir at the upstream inflow of the Maroon River and at five locations across the reservoir (Fig. 1c) for a limited time interval. These data were measured using RBR logging sensors moored at stations R, St1, St2, St3, St4 and St5 (Fig. 1c) in the

hypolimnion at 2 m above the bottom. The sensors were deployed in the flooding season between December 2011 and April 2012 (Mehrabani *et al.*, 2013). The recorded water temperatures at station R were used for the inflow boundary conditions and those from St1 through St5 for comparisons with the model's results.

Model description and setup

Model description

The Aquatic Ecosystem Model AEM3D (Hodges and Dallimore, 2016) is a three-dimensional hydrodynamic and ecosystem model for estuaries, lakes and reservoirs, and allows to predict water temperature, salinity, nutrients and biota variations in space and time. AEM3D uses the unsteady Reynolds-Averaged Navier-Stokes (RANS) and scalar transport equations with the Boussinesq and hydrostatic approximations. This model is an improved version of the ELCOM (Hodges, 2000) hydrodynamic and CAEDYM (Hipsey *et al.*, 2006) ecosystem models. Here we only use the hydrodynamic module of the model, as the focus is only on an analysis of the physical processes of the Maroon reservoir.

In AEM3D, the typical *k-ε* or eddy viscosity turbulence models (*e.g.*, see Zamani and Koch, 2020) are substituted with a standalone 3D vertical mixing model (Hodges *et al.,* 2000) to predict the wind-mixed layer depth and a model to more precisely model the distribution of momentum over the depth. The latter, being separately applied in the x and y directions, provides a direct increase in the velocity field of the wind-mixed layer before the Navier–Stokes equations are solved. A detailed description of the equations solved in AEM3D and further explanations of the underlying theory are provided in Hodges (2000) and Hodges *et al.* (2006).

AEM3D uses a modified adaptation of the TRIM-3D approach of Casulli and Cheng (1992) as its numerical scheme. The solution grid is a rectangular Cartesian grid with fixed longitudinal and lateral grid dimensions horizontally (Δx and Δy) and a vertical Δz spacing which is horizontally uniform but can vary in vertical dimension (*e.g.* different vertical layer thicknesses). The grid stencil is based on Arakawa's C-grid (Arakawa and Lamb, 1977) in which velocity vector values are defined on cell faces and scalar values (*e.g.* concentrations) on cell centers. The TRIM-3D approach is a semi-implicit finite difference method that numerically solves the 3D shallow-water equations for stratified flows.

Model setup and parameters

The AEM3D model allows the inclusion of Coriolis rotational effects, which are important for some large lakes/reservoirs. However, using this feature substantially increases the computational execution time and should

only be used when warranted. Coriolis is *generally* considered significant when the Rossby radius of deformation L_R (Wüest and Lorke, 2003) is less than the lateral length scale of the system. The L_R is computed as the ratio of inertial- to Coriolis forces:

$$L_R = \frac{C_I}{f} \qquad \text{eq. 1}$$

where is the phase speed of internal gravity waves given by $C_I = (g'D)^{(1/2)}$, with g' the reduced gravity due to stratification, D the water depth and f the Coriolis parameter. Using eq. (1) with appropriate parameters D and f for the Maroon reservoir, the Rossby radius L_R is calculated as 11000m, which is larger than the lateral dimensions (4000-5000m) of the main basins. Thus, the standard approach indicates that the Coriolis force can be safely neglected in modeling the Maroon reservoir. However, a recent study by Amadori *et al.* (2019) argued that the Rossby radius criterion is only valid for investigating the Coriolis effect for inertial currents and barotropic and baroclinic waves, whereas the Ekman

number could be a more important criterion for evaluating the Coriolis effect for wind-induced steady circulation. To date, tests of their hypothesis are limited to steady-state simulations in a one-dimensional and rectangular (with flat bottom) domain, and thus it is not clear whether it should apply to complex morphometry in a 3D basin with unsteady wind and flow conditions. To evaluate the relevance of the arguments of Amadori *et al.* (2019) to the present work, we performed a matched set of one-month-long simulations of the Maroon Reservoir with Coriolis both on and off. The differences between these two simulations had a root-mean-square error (RMSE) of 0.12°C. Furthermore, there were no significant differences in mean values (P=0.004). Thus, we argue that Coriolis forcing can be neglected for the Maroon reservoir's hydrodynamics and the Ekman number hypothesis of Amadori *et al.* (2019) requires further evidence for its extension to complex morphometry and unsteady forcing.

For the model grid of the Maroon reservoir a horizontal cell size of $\Delta x=\Delta y=100$ m, as shown in Fig. 1c, was used. In the vertical, layers have a uniform
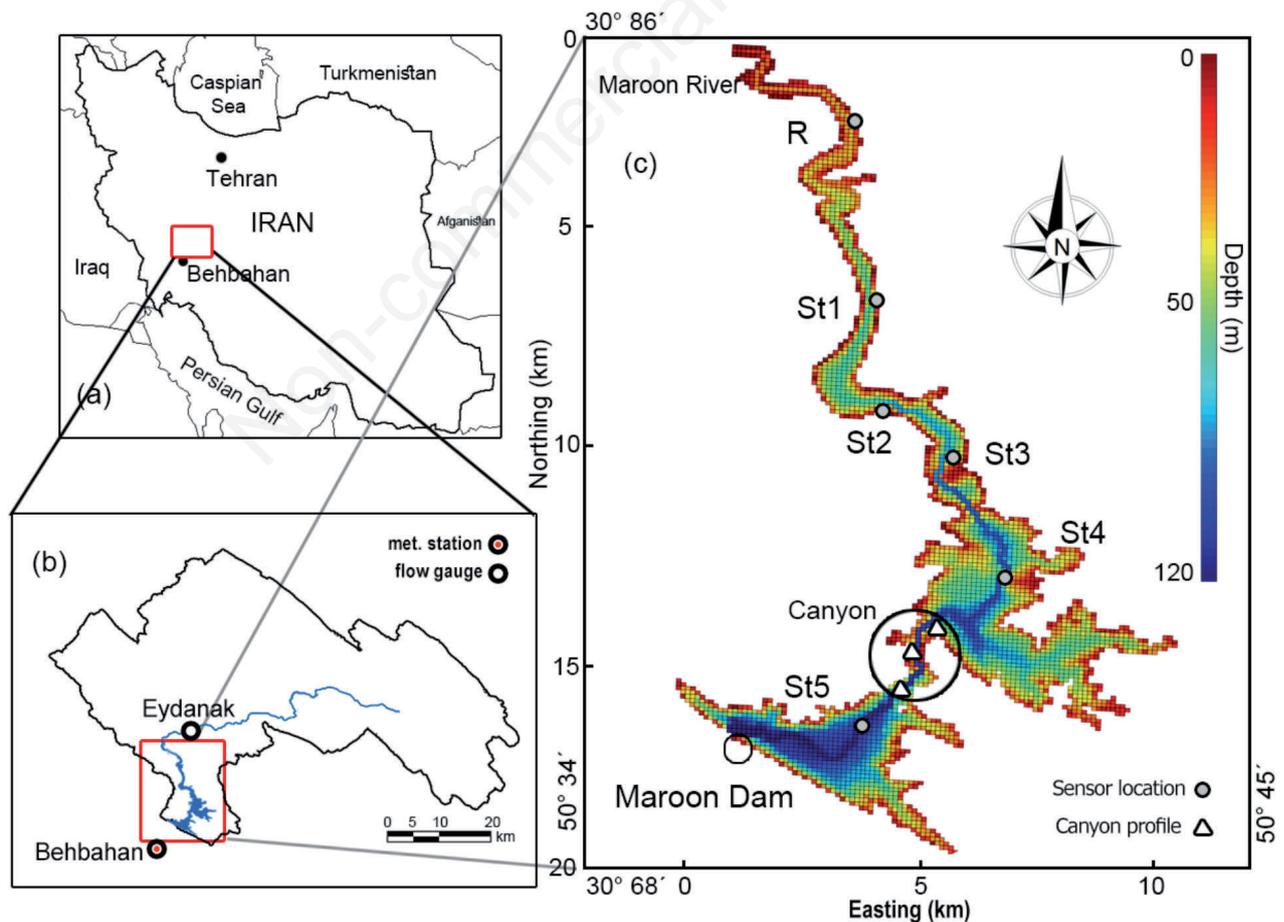
Fig. 1. a) Location of the Maroon reservoir. b) Maroon reservoir catchment and the location of the Behbahan meteorological station. c) AEM3D model grid with bathymetry of the Maroon reservoir with the canyon and sensor locations.

The Wedderburn Number (Imberger and Patterson, 1990) is defined as:

$$W = \frac{g' h_1^2}{u_*^2 L} \qquad \text{eq. 4}$$

where g' is the reduced gravity, *i.e.* $g' = g \, \Delta \rho \, \rho^{-1}$ where $\Delta \rho$ is the density difference across the thermocline, h_1 is the upper layer thickness, L is the fetch length, and u_*^2 is the wind stress which is computed from the wind speed as follows:

$$u_*^2 = C_d \left(\frac{\rho_a}{\rho_w} \right) W^2 \qquad \text{eq. 5}$$

where C_d is the wind stress coefficient (Tab. 1), ρ_a is the air density, ρ_w is the water density and W is the wind speed.

The Lake Number is calculated as (Imberger and Patterson, 1990; Robertson *et al.*, 1994):

$$L_N = \frac{S_t \left(1 - \frac{z_T}{z} \right)}{\rho_0 \, u_*^2 \, A_m^{3/2} \left(1 - \frac{z_g}{z} \right)} \qquad \text{eq. 6}$$

where z_g is the location of the lake's center of volume, z_T is the height to the center of the metalimnion (thermocline height), z_0 is the center of gravity of the water mass with a density stratification $r(z)$ at height z above the lake bottom, M is the total mass of the water, A_m is the surface area of the lake at the maximum height and g is the acceleration of gravity ($m \, s^{-2}$).

The Schmidt stability term S_t (J m^{-2}) (Schmidt, 1928; Hutchinson, 1957) that defines the work needed for mechanically mixing the entire water body into a uniform density distribution without any heat exchange is calculated as follows:

$$S_t = \frac{g}{A_M} \int_0^{z_m} (z - z_g) A_z (1 - \rho_z) dz \qquad \text{eq. 7}$$

where z is the height above bottom (cm), A_M is the lake surface area (cm^2) at the maximum height, A_z is the lake surface area (cm^2) at the height of z, and ρ_z is the water density (g cm^{-3}) at height of z. The three quantities mentioned above were calculated from the model results for the Maroon reservoir using the *Lake Analyzer* MATLAB toolbox (Read *et al.*, 2011).

RESULTS

Model validation and robustness analysis

Statistical results of the model validation for the water temperature are shown in Tab. 2. Overall, a good consistency between simulated (using the parameters' literature values of Tab. 1 without site-specific calibration) and observed temperatures is noticed. The AME and RMSE at the five stations are below 1°C, with the exception of the RMSE at St4, which is only slightly above 1°C. The overall temperature range is 11-16°C (Fig. 2) so we argue the model-observations are in reasonable agreement relative to this range. Note that this level of error is lower than that of some previously-published studies (Chung *et al.*, 2009; Lindim, 2010).

Continuous plots of the simulated and measured temperatures are shown in Fig. 2. Recall that the measured values at each station are taken at 2 m above the bottom and, hence, the large temperature falls observed in the various station plots of Fig. 2 are the consequence of the arrival of a cold-water density underflow in the wake of the two named flood events. To evaluate the modelled-observed data differences, note that the model values at a computational cell represent a volume of ~10^4 m^3, whereas the measurements at a sensor point represent less than 1 cm^3. This means that some differences are to be expected even for a perfect model. An overall good agreement between the temperature trends for all stations can be seen in Fig. 2. In contrast, we observe discrepancies for the large flood events, which increase from upstream station St1 to downstream station St5, and cannot simply be attributed to the difference between sensor volumes and model cell volumes.

Flood propagation analysis

Vertical profiles for the five months of simulated water column temperatures at the observation locations are shown in Fig. 3. The pathways of the two major flood events on January 14 and February 2 are shown in Fig. 4 and Fig. 5, respectively. A turbulent and relatively mixed water column exists in the transition zone, characterized by stations St1 – St3 (Fig. 3 b-d), where the advective

Tab. 2. Statistical results of the AEM3D temperature validation (°C).

Station	Mean (simulated)	Mean (observed)	AME	RMSE
St1	14.96	14.27	0.82	0.97
St2	14.48	14.57	0.41	0.71
St3	14.97	14.59	0.65	0.81
St4	13.98	14.19	0.88	1.07
St5	13.08	13.05	0.71	0.91
		mean	0.70	0.89

downslope propagation of the flood is the dominant factor in pushing the density current forward. The first flood event entering the reservoir was on January 14 (~150 m³ s⁻¹) and propagated as an underflow into the upper basin. This underflow took approximately 10 days to reach the downstream dam wall (Fig. 4), with an average propagation speed of 0.042 m s⁻¹. The minimum temperature of the current front at the river inflow point was 11.6°C while the density current front temperature reaching the dam wall was 14.5°C, showing the effect of initial mixing and entrainment of ambient waters during the transit. Initial mixing is the cumulative mixing happening in the vicinity of the plunge point where the river channel flow changes to a stratified flow. Entrainment of the ambient water into the current occurs by the turbulence generated from both interfacial shear and the bottom roughness affecting the density current

(Ford and Johnson, 1983; Hürzeler *et al.,* 1996; Scheu *et al.,* 2018). The reservoir was strongly affected by the second large flood on February 2, when the momentum of the inflowing density current (with a 9°C inflow temperature) dominated the buoyancy in the transition zone and mixed the entire water column during the peak of the flood event. After the density current passed through this zone, the water column remained nearly mixed for roughly three days (Fig. 5). Then the buoyancy forces dominated the weakened current during the recession limb of the flood hydrograph, pushing the mixed zone back, until the temperature stratification status came to an equilibrium within 10 days (Fig. 3 c,d). Further downstream, as the underflow transited into downstream (St4 to St5), buoyancy forces dominated and turbulence was suppressed by stratification. At station St4 the density current was seen to arrive as a bore that is rapidly
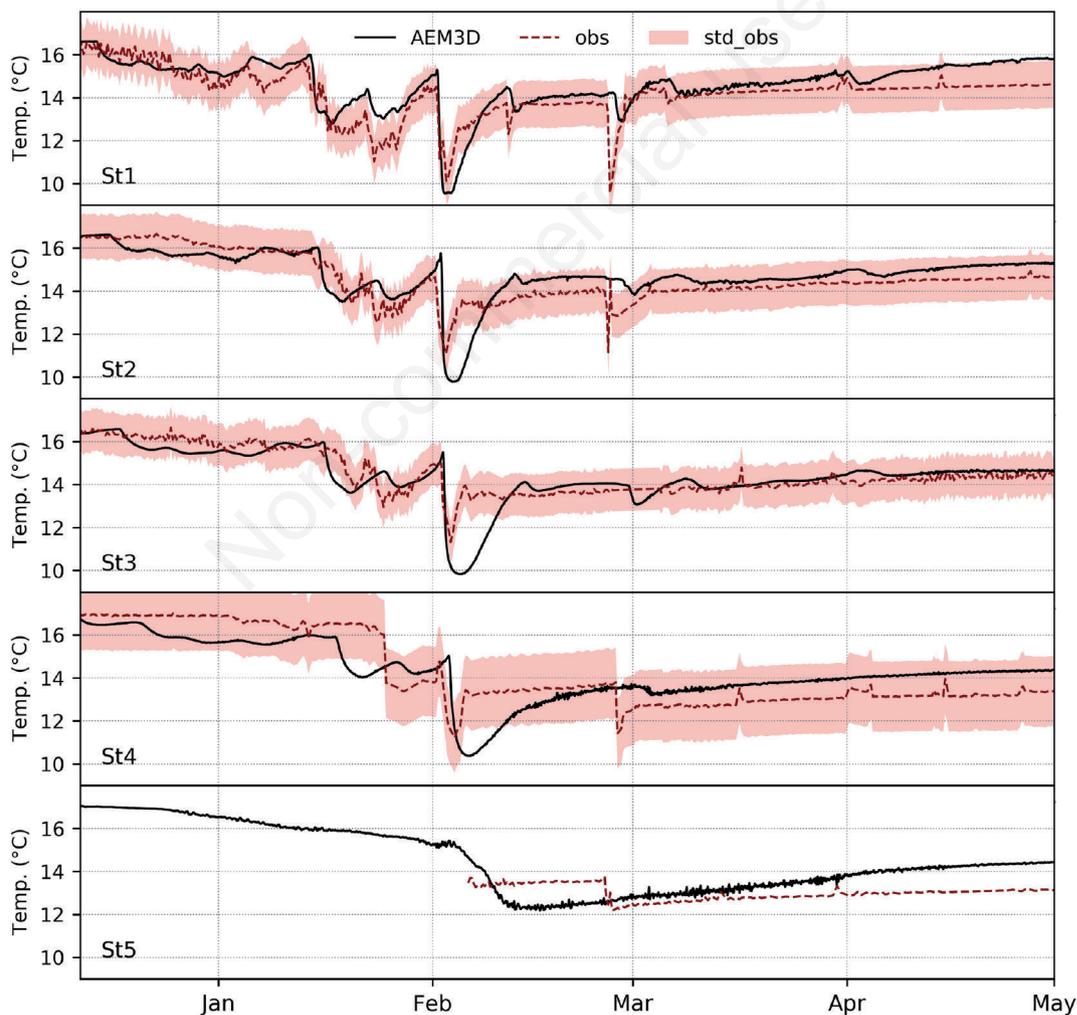
Fig. 2. Simulated (black line) water temperature at the measurement stations versus the measured values (red dashed line) at 2 m above bottom at each station. The light red bands denote the standard deviation of measured data. Note that the measured data for St5 are only available for February and later.

dissipated in the deepest sections which manifests itself in the form of some oscillations of the 14°C temperature contour, indicating the existence of internal waves propagating through the system. On the other hand, at the most downstream station St5 in the lower basin the dense current fills the lacustrine zone completely and slowly
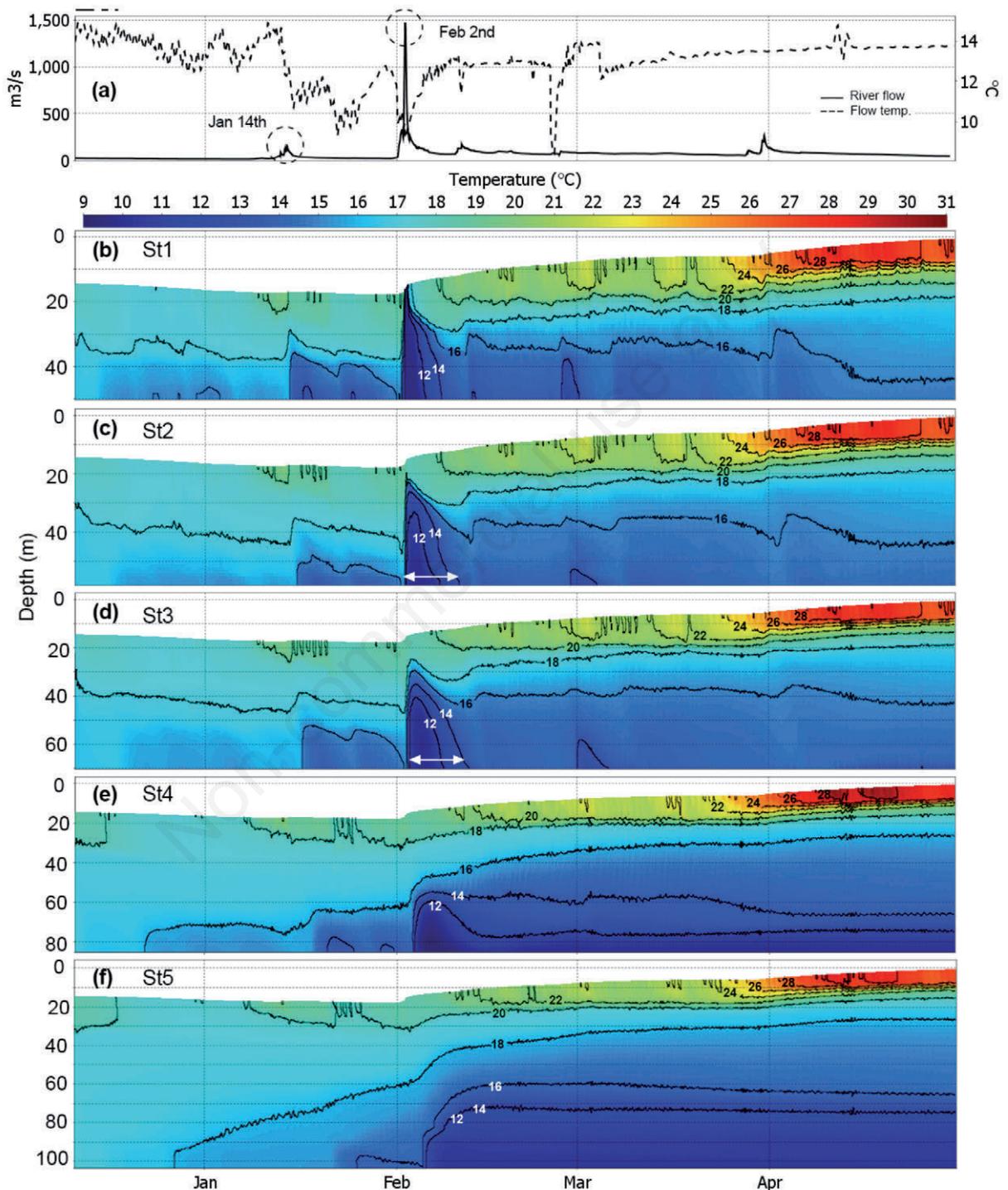
Fig. 3. a) Measured river inflow rate (continuous line) and temperature (dashed line) into the Maroon reservoir; temporal variation of the simulated water temperature by AEM3D as hourly profiles of water column temperature at (b), (c) and (d) transitional zone, (e) upper lacustrine zone and, (f) lower lacustrine zone. The white arrows show the 10 days period after the February 2nd flood in the transition zone (see text for more information).

Fig. 6. Wedderburn number (a), Lake Number (b) and Schmidt stability (c), calculated for the AEM3D simulation period (2011-12). Discontinuous time series of *LN* and *W* are due to having no wind on the corresponding days.
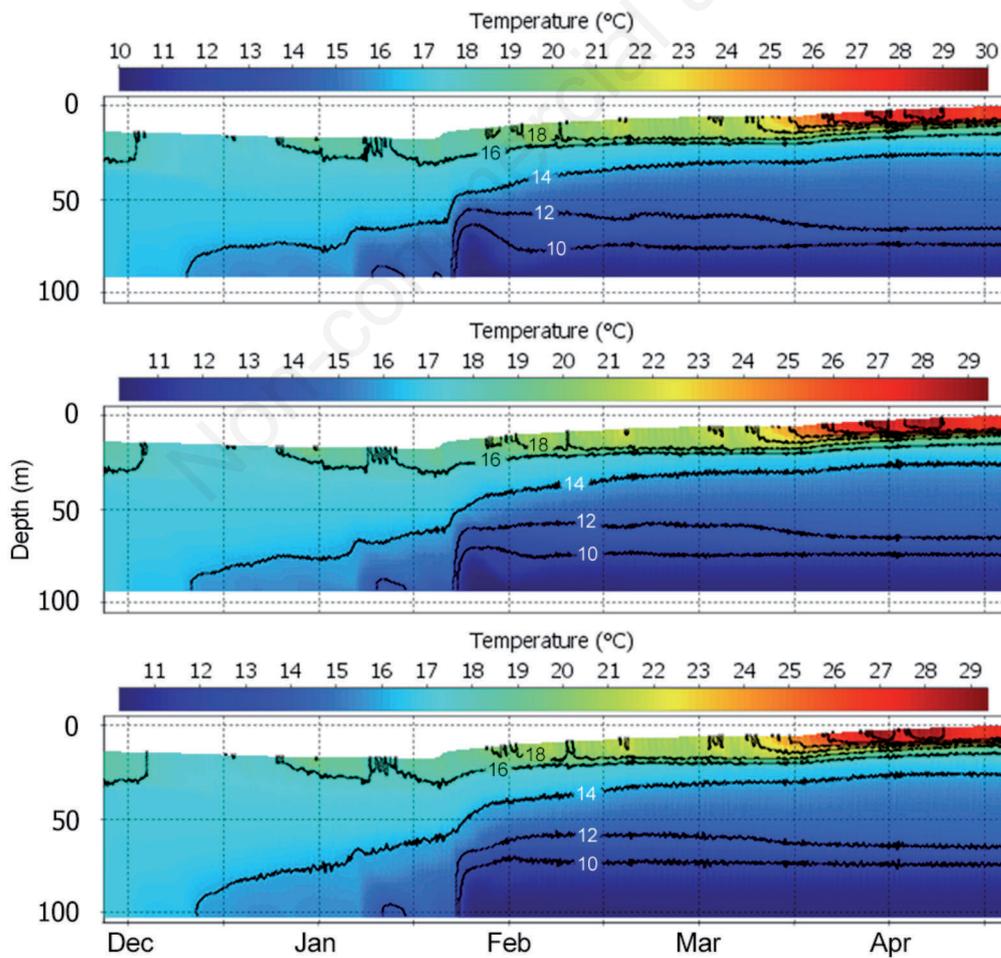
Fig. 7. Simulated water column profiles of the canyon connecting the two basins of the Maroon reservoir: (a) upstream of the canyon, (b) middle of the canyon, and (c) downstream of the canyon.

above in reference to Fig. 3) never sees a strong effect of the density current. Instead, a relatively consistent large L_N throughout the period is obtained, with W being initially large and variable, then dropping rapidly in April with the onset of epilimnion warming by atmospheric forcing. The large L_N indicates that the lake in the lower basin remains stratified while the decreasing W is evidence that the lake response to wind forcing is mainly in the epilimnion and does not significantly affect the thermocline or hypolimnion. Once W drops below unity, the baroclinic restoring force reaches a sufficiently strong level to limit the surface mixing to the upper 4 m of the water column.

The analysis above is consistent with the evolution of S_t in the upper and lower basins (Fig. 6c). At the onset of the simulation, both basins begin with relatively low stability as there is not much solar radiation forcing of the lake's surface in the wintertime. As time goes on, the upper basin S_t shows a small increase with the propagation of the density plume and then settles down to a smaller value than the S_t of the lower basin. The smaller value of S_t in the upper basin is consistent with the higher center of gravity (z_g) of the cross-sections in this shallower region of the reservoir. In contrast, the S_t of the lower basin is steadily increasing over time, associated initially with the inflow of colder water and then later with the increasing spring temperature in the epilimnion. These findings are consistent with the temperature profiles of St4 (upper basin) and St5 (lower basin) as discussed above for Fig. 3.

Hydrodynamic effects

The hydrodynamic processes in the narrow canyon connecting the two basins of the Maroon reservoir can be noticed from the anomalies of three simulated temperature profiles in Fig. 7, taken at three locations (shown in Fig. 1c), and are separated by a distance of 1000 m. The most upstream profile (Fig. 7a) shows the strong arrival of the head of the density current, similar to what occurred at station St4 in the upper basin (Fig. 3e), whereas the most downstream profile (Fig. 7c) exhibits the simple filling behavior by cold water in the hypolimnion, similar to what has been observed at station St5 in the lower basin (see Fig. 3). The central canyon profile (Fig. 7b) represents clearly a transition between the two sections named.

A more quantitative picture of the processes occurring in the narrow canyon is presented in Fig. 8 which shows the time series of the temperature anomalies (temperature relative to the mean) at three discrete levels of the water column in the three canyon sections. These anomalies show clearly the signatures of the underflow at the upper and middle canyon sites at 15 and 30 m above the bottom, whereas at the downstream site only a very small signature of the density current is seen at 15 m above the bottom, indicating that by then the current has slowed and spread. This transition from the upper-basin behavior to the simple filling behavior of the density current in the narrow canyon is also seen in Fig. 5 discussed earlier where the contours do not follow the bottom topography through the canyon and a sharp downward bending of the temperature contours occurs in the hypolimnion therein.
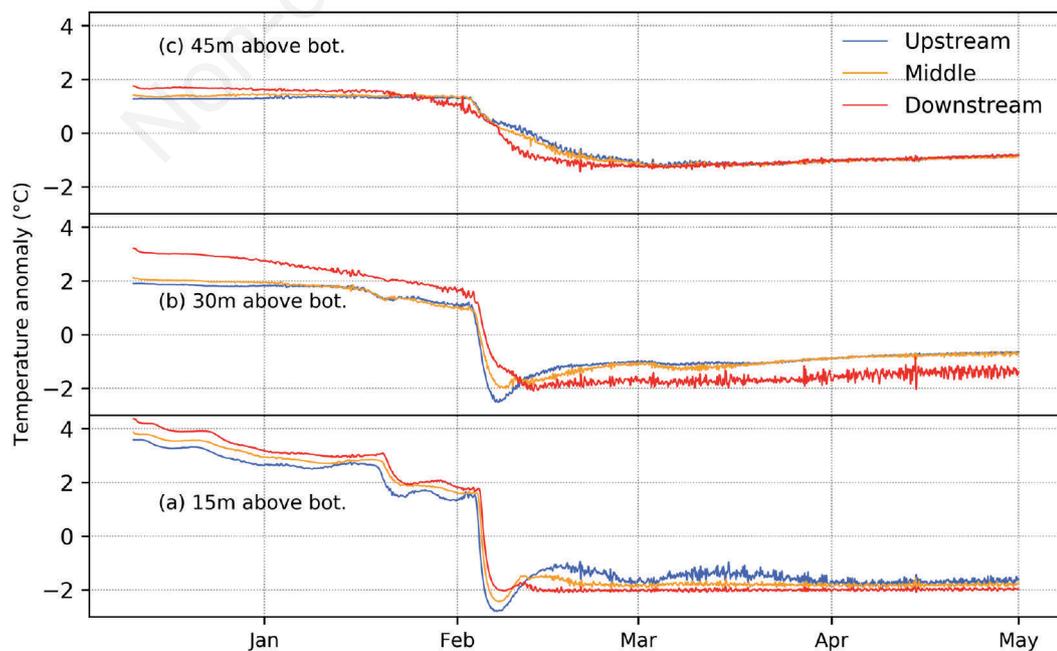

Fig. 8. Anomalies of water temperature at selected elevations of upstream, middle and downstream of the canyon.

Secondly, the 100×100×1 m numerical model grid is relatively coarse for properly representing the reservoir's thalweg, as the steep valley morphometry is actually narrower near the bottom than the grid size over much of the domain, especially in the zones upstream of station St4 and in the canyon connecting the upper and lower basins. This coarse-grid effect occurs predominantly in the lower two or three grid cells (which includes the model-data comparison points) and results in a broader cross-sectional area for the model hypolimnion. The misrepresentation of the cross-sectional area in the thalweg will affect the overall thickness of a propagating density plume as well as its speed and mixing.

A third likely source of error is the mechanism proposed by Hodges *et al.* (2006) who showed that models using the hydrostatic approximation (as AEM3D herein) lead, in the presence of large nonlinear internal waves, to a bias that alters the modeled wave propagation. This typically results in excessive steepening of the front of a model internal wave, as appears to be the case in Fig. 2.

Although refining the model grid would undoubtedly help to resolve the under-resolution problem (2) for the thalweg, a key point of Hodges *et al.* (2006) is that grid refinement cannot remove the underlying bias associated with the neglect of the non-hydrostatic terms. Instead, refining the grid merely changes the balance between numerical dissipation and numerical dispersion (oscillation) at the wave front, typically leading to waves with greater artificial steepening. In the limit, grid refinement of a hydrostatic model is merely a better solution of the wrong equations and is not necessarily a better representation of the real world. This observation, while somewhat bleak, is actually quite helpful. Instead of wasting more computational time on finer grids, we can simply ask whether our hydrostatic model, while being "wrong" in the sense of Box (1976), is also "useful". For the present purposes, Fig. 2 shows reasonable agreement between modeled and observed water temperatures across all of stations over the five-month simulation horizon. The key density current events occur with similar scales and timing (*e.g.*, rapid cooling in February) and the statistical analyses (Tab. 2) provide further validation. Therefore, the AEM3D hydrodynamic model achieves overall good agreement with the observations, using parameters based solely on literature values. Consequently, this work provides further evidence that 3D state-of-the-art modeling is able to provide valuable insights into various physical reservoir processes, namely, the hydrodynamics of the density currents, and this is accomplished without requiring extensive calibration data.

CONCLUSIONS

This study presents the application of an uncalibrated 3D hydrodynamic model to the Iranian Maroon reservoir.

Our study shows the important role which the morphology of the reservoir plays in controlling the hydrodynamics in a way that alters the limnological character of the two reservoir basins connected by a narrow canyon. The cold density currents during the winter/spring floods are shown to propagate rapidly through the upper basin but are moderated by the narrow canyon separating the upper and lower basins.

The analysis evaluated the response of the two basins to wind forcing in terms of the Lake Number (L_N), Wedderburn number (W) and the Schmidt stability term (S_t). The results indicate that the upper basin is less stable than the downstream one (despite stronger stratification of the underflow) and is more prone to mixing by both wind and a flowing gravity current (cold plume in the wake of the two flood events). The lower basin is more stable and the main response to wind forcing is limited to mixing in the epilimnion.

The analysis of the canyon hydrodynamics shows further that the narrow constriction is effectively partitioning the reservoir into two basins with different stratification and mixing behaviors. At the downstream section of the canyon, the background potential energy (BPE), after the passing of each density current (after the recession limb of the two flood events) shows higher values than those before the flood, whereas the opposite is observed for the upstream section of the canyon. These differences are even more prominently visible from the Schmidt stability values (S_t) of the up- and downstream sections of the canyon. Due to stronger mixing processes, S_t for the upstream canyon section initially decreases and undergoes a rapid increase due to the flood events' bore flow, but then steadily regains its pre-flood value. In contrast, the S_t for downstream canyon section (and that of the lower basin) continues to increase due to increased stratification by the spring seasonal heating in the epilimnion.

From this analysis we are able show the canyon morphology in the Maroon reservoir dissipates the sharp front of the flood bore as it propagates downstream into the lower basin during the two flood events. These effects are reflected in the stratification and mixing behaviors that, in turn, may affect the evolution of reservoir's water quality over seasonal timescales.

The reservoir morphology clearly affects the overall energy balance and the fate of density currents, which are important factors in the sedimentation within the reservoir. It follows that future studies should examine suspended solids and turbidity, whose distribution may be affected by the propagation and dissipation of the flood underflows. However, to do so properly, long-term observations with thermistor chains that cover the full depth of the lake are needed. Furthermore, additional sensors upstream and downstream at the entrance and exit

to the canyon would be particularly valuable for future modeling.

REFERENCES

Alizadeh A, Khalili N, 2009. [Estimation of Angstrom coefficient and developing a regression equation for solar radiation estimation (case study: Mashhad)].[Article in Persian]. J. Water Soil 23:229-238.

Allen RG, Pereira LS, Raes D, Smith M, 1998. Crop Evapotranspiration – Guidelines for Computing Crop Water Requirements. FAO Irrigation and drainage paper 56. Food and Agriculture Organization of the United Nations, Rome.

An S, Julien PY, 2014. Three-dimensional modeling of turbid density currents in Imha Reservoir, South Korea. J. Hydraul. Eng. 140:05014004.

Amadori M, Piccolroaz S, Dijkstra HA, Toffolon M (2019). What makes an elongated lake 'large'? Scales from wind-driven steady circulation on a rotating Earth. J. Great Lakes Res. (in press). doi: 10.1016/j.jglr.2019.10.013.

Ångström A, 1924. Solar and terrestrial radiation. Q. J. R. Meteorol. Soc. 50:121-125.

Antenucci JP, Imberger J, 2001. Energetics of long internal gravity waves in large lakes. Limnol. Oceanogr. 46:1760-1773.

Arakawa A, Lamb VR, 1977. Computational design of the basic dynamical processes of the UCLA general circulation model, p. 173-265. In: Chang J. (ed.), General Circulation Models of the Atmosphere. Methods in Computational Physics. Elsevier.

Botelho Daniel A, Imberger J, 2007. Dissolved oxygen response to wind-inflow interactions in a stratified reservoir. Limnol. Oceanogr. 52:2027-2052.

Box GEP, 1976. Science and statistics. J. Am. Stat. Ass. 71:791-799.

Bourent PE, Dartus D, Tassin B, Vincon-Leite B, 1999. Numerical investigation of plunging density current. J. Hydraul. Eng. 125:584-594.

Cassulli V, Cheng RT, 1992. Semi-implicit finite difference methods for three-dimensional shallow water flow. Int. J. Numer. Meth. 15:629-648.

Chung SW, Hipsey MR, Imberger J, 2009. Modelling the propagation of turbid density inflows into a stratified lake: Daecheong Reservoir, Korea. Environ. Model. Softw. 24:1467-1482.

Cortés A, Fleenor WE, Wells MG, de Vicente I, Rueda FJ, 2014. Pathways of river water to the surface layers of stratified reservoirs. Limnol. Oceanogr. 59:233-250.

Ford DE, Johnson LS, 1986. An assessment of reservoir mixing processes, technical report for US Army Corps of Engineers. Ford Thornton Norton and associates Ltd., USA.

Hajjam S, Jamei M, 2009. [Estimation of solar radiation parameter (sunshine hours) and Angstrom coefficients in Khuzestan Province].[Article in Persian]. Proceedings 10th National Conf. of Irrigation and Evaporation Reduction, Kerman, Iran.

Hamilton, DP, Schladow, SG, 1997. Prediction of water quality in lakes and reservoirs: Part I-Model description. Ecol. Model. 96:91-110.

Hayes NM, Deemer BR, Corman JR, Razavi R, Strok KE, 2017. Key differences between lakes and reservoirs modify climate signals: A case for a new conceptual model. Limnol. Oceanogr. Lett. 2:47-62.

Hipsey MR, Antenucci JP, Brookes JD, 2008. A generic, process-based model of microbial pollution in aquatic systems. Water Resour. Res. 44:W07408. doi: 10.1029/2007WR006395.

Hodges BR, Dallimore C, 2016. Aquatic Ecosystem Model: AEM3D, User manual. Hydronumerics, Australia.

Hodges BR, Imberger J, Saggio A, Winters KB, 2000. Modeling basin-scale internal waves in a stratified lake. Limnol. Oceanogr. 45:1603-1620.

Hodges BR, Laval B, Wadzuk BM, 2006. Numerical error assessment and a temporal horizon for internal waves in a hydrostatic model. Ocean Model. 13:44-64.

Hogg CAR, Dalziel SB, Huppert HE, Imberger J, 2017. Inclined gravity currents filling basins: the impact of peeling detrainment on transport and vertical structure. J. Fluid Mech. 820:400-423.

Hutchinson GE, Loffler H, 1956. The thermal classification of lakes. P. Natl. Acad. Sci. 42:84-86.

Hutchinson GE, 1957. A treatise on limnology. J. Wiley & Sons, Inc., New York.

Hürzeler BE, Imberger J, Ivey GN, 1996. Dynamics of turbidity current with reversing buoyancy. J. Hydr. Engin. 122:230-236.

Imberger J, Patterson JC, 1990. Physical limnology. Adv. Appl. Mech. 27:303-475.

Ji Z-G, 2008. Hydrodynamics and water quality: modeling rivers, lakes, and estuaries. J. Wiley & Sons, Inc., New York.

Jørgensen SE, Löffler H, Rast W, Straškraba M, 2005. Lake and reservoir management. Elsevier Inc.

Kennedy RH, Thornton KW, Ford DE, 1985. Characterization of the reservoir ecosystem. In: D. Gunnison (ed.), Microbial Processes in Reservoirs. Springer.

Kim, Y. and B. Kim. 2006. Application of a 2-dimensional water quality model (CE-QUAL-W2) to the turbidity interflow in a deep reservoir (Lake Soyang, Korea). Lake Reserv. Manage. 22:213-222. https://doi.org/10.1080/07438140609353898.

Lindim Fontes C, 2010. Modelling of water quality in the Alqueva Reservoir, Portugal. PhD thesis, University of Minho, Portugal.

Löffler H, 2004. The origin of lake basins, p. 8-60. In: P.E.

O'Sullivan and C.S. Reynolds (eds.), The lakes handbook. Blackwell Publishing.

Marti CL, Imberger J, Garibaldi L, Leoni B, 2016. Using time scales to characterize phytoplankton assemblages in a deep subalpine lake during the thermal stratification period: Lake Iseo, Italy. Water Resour. Res. 52:1762–1780.

Mehrabani R, Makvandi A, Nekouyanfar M, Hassounizadeh H, 2013. Tracing and measurement of turbidity current in maroon dam. Proceedings 9th Int. River Engineering Conf., Ahwaz, Iran.

Panse S, 2013. Background and available potential energy in numerical simulations of a Boussinesq Fluid. Master's Thesis 1911 - February 2014. 1002.

Read JS, Hamilton DP, Jones ID, Muraoka K, Winslow LA, Kroiss R, Wu CH, Gaiser E, 2011. Derivation of lake mixing and stratification indices from high-resolution lake buoy data. Environ. Model. Softw. 26:1325-1336.

Robertson DM and Imberger J, 1994. Lake Number, a quantitative indicator of mixing used to estimate changes in dissolved oxygen. Int. Revue Ges. Hydrobiol. 79: 159-176.

Rueda FJ, McIntyre S, 2010. Modelling the fate and transport of negatively buoyant storm–river water in small multi-basin lakes. Environ. Model. Softw. 25:146-157.

Scheu KR, Fong D, Monismith SG, Fringer OB, 2018. Modeling sedimentation dynamics of sediment-laden river intrusions in a rotationally-influenced, stratified lake. Water Resour. Res. 54:4084- 4107.

Schladow SG, Hamilton DP, 1997. Prediction of water quality in lakes and reservoirs: Part II-Model calibration, sensitivity analysis and application. Ecol. Model. 96:111-123.

Schmidt W, 1928. [Ueber Temperatur and Stabilitaetsverhaltnisse von Seen].[Article in German]. Geographiska Annaler 10:145-177.

Thornton JA, Rast W, Steele A, 1996. Reservoirs. In: D. Chapman (Ed.), Water Quality Assessments, 2nd Ed. Chapman and Hall, London, 369-412.

USACE U.S. Army Corps of Engineers, 1987. Reservoir water quality analysis, Engineer Manual. USA.

Valerio G, Pilotti M, Marti CL, Imberger J, 2012. The structure of basin-scale internal waves in a stratified lake in response to lake bathymetry and wind spatial and temporal distribution: Lake Iseo, Italy. Limnol. Oceanogr. 57:772-786.

Vincent WF, Gibbs MM, Spigel RH, 1991. Eutrophication processes regulated by a plunging river inflow. Hydrobiologia 226: 51-63.

Winters K, Lombard P, Riley J, D'Asaro E, 1995. Available potential energy and mixing in density-stratified fluids. J. Fluid Mech. 289:115-128. doi:10.1017/S002211209500125X.

Wüest A, Lorke A, 2003. Small-scale hydrodynamics in lakes. Annu. Rev. Fluid Mech. 35:373-412. doi: 10.1146/annurev. fluid.35.101101.161220.

Yang K, Koike T, 2005. A general model to estimate hourly and daily solar radiation for hydrological studies. Water Resour. Res. 41:W10403. doi: 10.1029/2005WR003976

Zamani B, Koch M, Hodges BR, Fakheri-Fard A, 2018. Pre-impoundment assessment of the limnological processes and eutrophication in a reservoir using three-dimensional modeling: Abolabbas reservoir, Iran. J. Appl. Water Engin. Res. 6:48-61. doi: 10.1080/23249676.2016.1209440.

Zamani B, Koch M, 2020. Comparison between two hydrodynamic models in simulating physical processes of a reservoir with complex morphology: Maroon Reservoir. Water 12:814.